

MUON BEAM DYNAMICS AND SPIN DYNAMICS IN THE G-2 STORAGE RING *

D. L. Rubin[†], A. Chapelain, Cornell University, Ithaca, USA
F. Grey, Regis University, Denver, USA
J. Price, University of Liverpool, Liverpool, UK
J. Mott, Boston University, Boston, USA
J. Crnkovic, W. Morse, Brookhaven National Laboratory, Upton, USA
V. Tishenko, University of Kentucky, Lexington, USA
W. Wu, University of Mississippi, Oxford, USA

Abstract

The goal of the new g-2 experiment at fermilab is a measurement of the anomalous magnetic moment of the muon, with uncertainty of less than 140 ppb. The experimental method is to store a beam of polarized muons in a storage ring with pure vertical dipole field and electrostatic focusing, and to measure the precession frequency. Control of the systematics depends on unprecedented knowledge of the details of the phase space of the muon distribution. That knowledge is derived from direct measurements with scintillating fiber detectors that are inserted into the muon beam for diagnostic measurements, traceback straw tube tracking chambers, as well as indirectly with the calorimeters that measure energy, time and position of the decay positrons. The interpretation of the measurements depends on a detailed model of the storage ring guide field, including nonlinearity of the electrostatic quadrupole fields, and magnetic field errors that we have developed. This invited talk presents results of studies of the distribution from the commissioning run of the experiment.

INTRODUCTION

The muon magnetic moment is a property that can be calculated in the context of the standard model. A comparison of the measured and predicted anomaly is a grand test of the standard model. A discrepancy would indicate new physics. The goal of the experiment is to measure the anomalous magnetic moment with 140 part per billion precision.

The experimental method is to circulate a beam of polarized muons in a storage ring and to measure the precession frequency, or rather the difference between the precession frequency and the revolution frequency, ω_a , that is, the spin tune. The 3.094 GeV momentum muons decay with lifetime of about 64 ns in the lab frame to a positron and a pair of neutrinos. The energy of the positron in the lab frame is correlated with the polarization of the parent muon. The variation in the number of high energy positrons with time is the measure of the difference frequency.

The frequency with which the muons precess depends on the details of the magnetic and electric guide field of the storage ring. Magnetic focusing is evidently precluded as it

would introduce an unacceptable variation in the magnetic field across the storage volume. Alternatively vertical focusing is provided by electro-static quadrupoles. The muon momentum is chosen to minimize the effect of the electric field on the precession frequency. Indeed, at the muon magic momentum, 3.094 GeV/c, the contribution of the electric field to the difference frequency vanishes.

We describe the electric and magnetic guide field of the 44.69 m circumference storage ring, the lattice functions and the process for injecting and storing polarized muons. The detector systems that inform the beam distributions are introduced. And the contributions to ω_a that arise from finite beam width and length, momentum spread, coherent oscillation of the centroid are described, as are the measurements of the distributions that are essential to accounting for the effects.

STORAGE RING

The g-2 storage ring is a weak focusing machine with a single adjustable parameter, namely the quadrupole voltage, that determines horizontal and vertical tunes, β -functions, and dispersion. Fig. 1 indicates the layout of the quadrupoles. The quads are vertically focusing and horizontally defocusing. In the limit where $V_{quad} \rightarrow 0$, the horizontal tune is unity and vertical is zero. With increasing voltage the vertical tune increases and horizontal decreases. Fig. 3 shows horizontal and vertical tunes along the voltage contour. Non-linearities associated with the electrostatic quadrupoles [5], as well as residual magnetic multipoles [1] can drive resonances, also shown in Fig. 3. Operation near such resonances is avoided to minimize the number of muons lost over the course of the fill. The β and dispersion functions for quad voltage of 20.2 kV are shown in Fig. 2.

The quadrupole field is superimposed on the main dipole field. The reference trajectory through the quadrupoles therefore has significant curvature and the quadrupoles share that curvature. As a result, the quadrupole field is necessarily nonlinear, with a significant sextupole term. An effect of this and other geometric nonlinearities is amplitude dependence of the tunes. The tunes shifts associated with the various quad multipoles [5] are shown in Fig. 8.

Calorimeters distributed around the inner circumference of the ring measure energy, position and time of decay

* Work supported by DOE DE-SC0008037

[†] david.rubin@cornell.edu

positrons. There are tracking stations at 180 and 270 deg. Each station is comprised of 8 modules with 128 straws in a module. The straw wire chambers measure the trajectory of the decay positron. The track can be extrapolated back to the position of the parent muon. The four fiber harps. Each harp consists of seven 0.5mm diameter parallel scintillating fibers with 13mm spacing. There are two horizontal and two vertically oriented harps at 180 and 270 degrees respectively. The fiber harps are flipped into the beam to give direct a measure of time dependence of beam centroid and profile.

The guide field is characterized by measurements of closed orbit, tunes, and modulation of the beam width and centroid. Measurements of the tunes with the fiber harps are shown in Fig. 4. The fiber harps and the tracking detectors provide complimentary measurements of motion of the centroid (Figs. 5 and 7) and modulation of the width, Fig. 6.

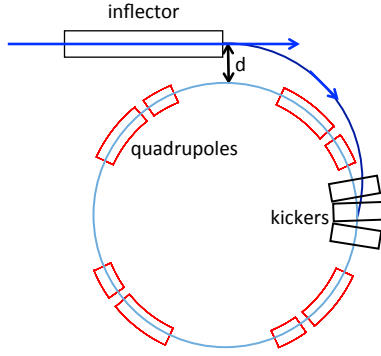


Figure 1: Injected beam enters the g-2 ring through a hole in the backleg iron. It emerges in from the backleg and enters the inflector which cancels the field of the g-2 magnet. Beam exits the inflector, and enters the ring through the kicker gap. The electrostatic quadrupoles vertically focus, horizontally defocus. The circumference of the ring is 44.69 m (revolution period 149 ns). The 1.45 T bending field is continuous around the ring.

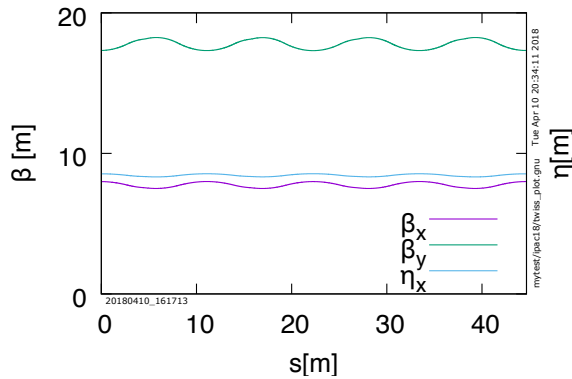


Figure 2: Twiss parameters of the closed storage ring

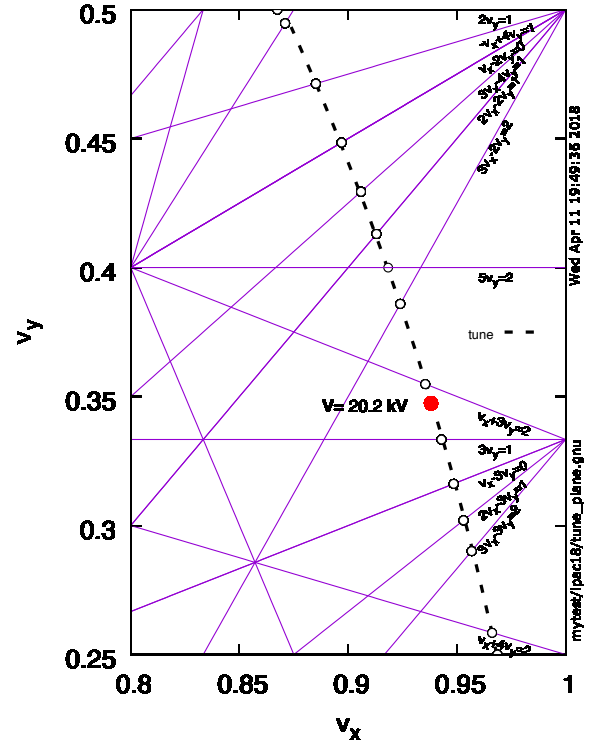


Figure 3: Dependence of tune on quadrupole voltage computed with a BMAD [2] based model of the guide field. Resonance lines are shown and a safe operating point, at 20.2 kV is indicated.

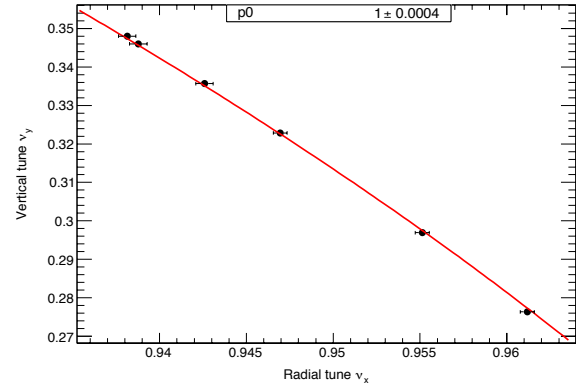


Figure 4: Measurement of the tunes with the fiber harps along the quadrupole voltage contour.

INJECTION

The beam is injected into the ring through a hole in the backleg iron. The final magnetic element in the injection channel is the 1.7m long superconducting inflector that bucks the main dipole field so that the beam exits the inflector on a trajectory tangent to a displaced circular orbit. The beam crosses the design orbit in the gap of the pulsed kicker that steers it onto the central orbit as shown in Fig. 1.

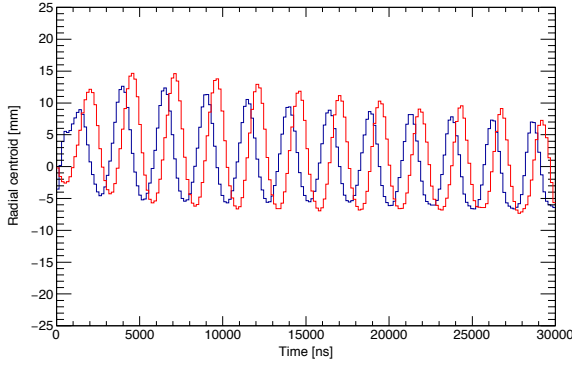


Figure 5: Horizontal position of centroid measured with the 180 deg fiber harp (blue) and 270 deg harp (red) for the first $30\mu s$ of the fill. An FFT yields the horizontal tune.

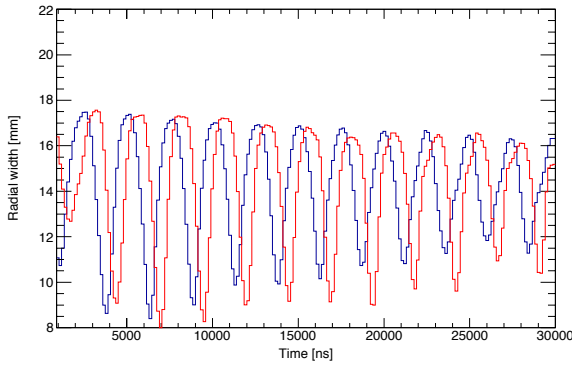


Figure 6: Horizontal width at 180 degree harp (blue) and 270 deg harp (red) over the first $30\mu s$ of the fill. An FFT has components at the fundamental and second harmonic of the horizontal motion corresponding to dispersive and β mismatch.

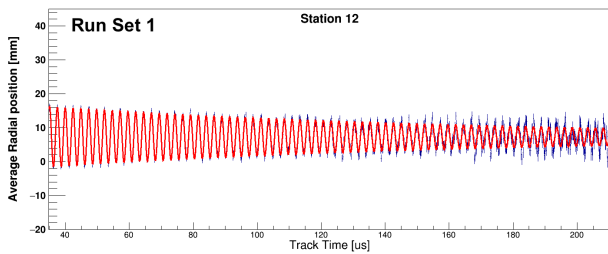


Figure 7: Vertical centroid as measured with the 180 deg tracker over the first $22\mu s$ of the fill,

The inflector aperture (18 mm horizontally by 56 mm vertically) is very much smaller than the aperture of the ring (90mm round). In order to maximize transmission, the beam is focused to a narrow waist through the inflector with zero dispersion.

Manipulation of the beam width to maximize transmission through the inflector and into the ring is shown in Fig. 10. The resulting mismatch of both β -functions and the dispersion is indicated in Fig. 9. The mismatch of dispersion

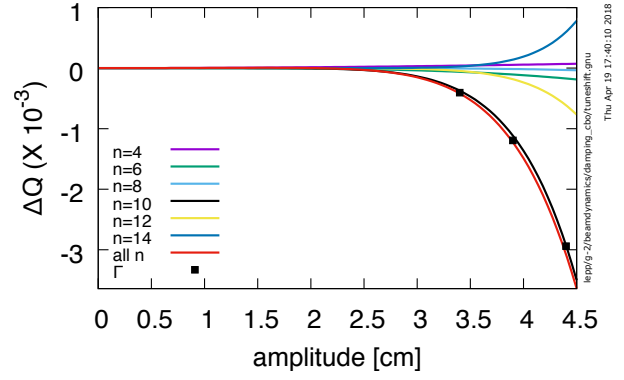


Figure 8: Contribution to amplitude dependent tune shift from each of the quad multipoles, their sum, and the decoherence rate as determined by tracking.

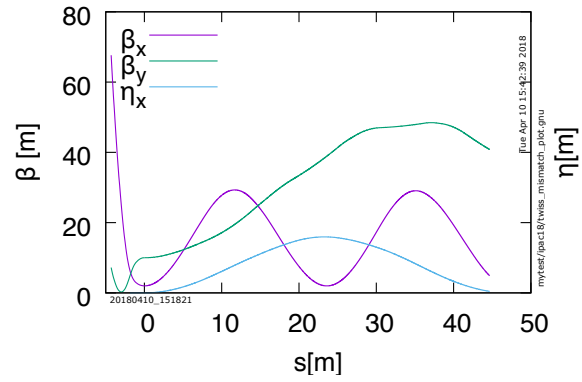


Figure 9: Propagating mismatched twiss parameters through the narrow aperture inflector and into the storage ring with quads at 20.2kV

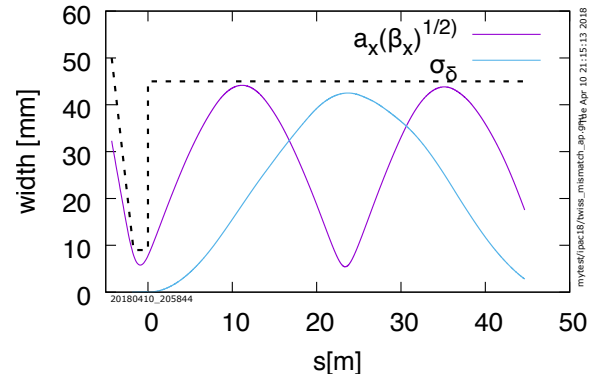


Figure 10: Propagating beam betatron and energy width through narrow aperture inflector and into the storage ring

and β -functions leads to a modulation of beam width with components at the betatron frequency and twice the betatron frequency respectively.

The kicker is located $\phi_\beta = \pi/2$ downstream from the injection point at the inflector exit. The beam crosses the design orbit with an angle determined by the radial displacement of the inflector axis (nominally 77 mm from the design

orbit and indicated as 'd' in Fig. 1) and the exit angle. The crossing angle, and therefore the kick required to steer the beam onto the closed orbit, is minimum if the exit angle is zero. The dependencies can be made quantitative with a few simplifying assumptions, namely that the β and η functions are uniform around the ring, and we treat the kickers as a δ -function in azimuthal angle. (The kickers [3] extend over about 36 deg of arc). Then the horizontal displacement of the trajectory is

$$\begin{aligned} x(s) &= (x_{inf} - \delta\eta) \cos(\phi(s)) + \eta\delta \\ &\quad - k\beta_0 \cos \phi(s) + x'_{inf} \sin \phi(s) \\ &= A \cos(\phi(s) + \phi_0) + \eta\delta \end{aligned}$$

where x_{inf}, x'_{inf} are the displacement and angle of the trajectory at the inflector exit, δ is the fractional momentum offset, k is the kick angle, $\phi(s)$ the betatron phase advance with $s = 0$ at the injection point, $A = \pm \sqrt{(x_{inf} - \delta\eta - k\beta)^2 + (x'_{inf}\beta)^2}$ and $\tan \phi_0 = \frac{x'_{inf}\beta}{x_{inf} - \delta\eta - k\beta}$. The extremes of the displacement of the motion, that is the envelope of the motion is given by $x_{ext} = \pm|A| + \eta\delta$. The envelope is plotted in Fig. 11 as a function of momentum for three different injection angles, and for a kick angle $k = 8\text{mrad}$, which is about 80% of the nominal kick. and Fig. 12 for the nominal kick of $k = 10.8\text{mrad}$. Evidently, the momentum acceptance and therefore the momentum distribution of the beam that is stored is largely determined by the effective kicker angle. Underkicking shifts the momentum distribution higher. The amplitude of the oscillations of muons about the closed orbit is largely determined by the injection angle.

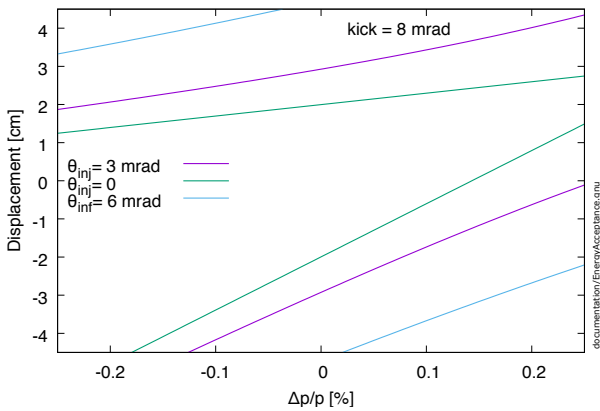


Figure 11: Kick angle $\sim 80\%$ of nominal. The green lines mark the envelope of the motion of a muon that exits the inflector with zero angle. The on momentum muon oscillates between ± 2 cm. If momentum offset is 0.2% the peak to peak oscillation is ~ 5 mm. A muon with momentum offset of -0.2% is outside the 4.5 cm aperture.

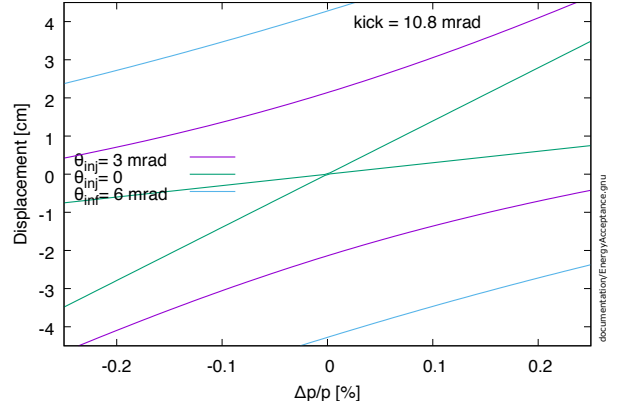


Figure 12: For the nominal kick angle (10.8 mrad), the trajectory of the on momentum muon coincides with the closed orbit. The on momentum muon injected with angle of ± 3 mrad will oscillate within a ± 2 cm envelope.

SYSTEMATICS

The expression for the anomalous precession frequency is given by

$$\begin{aligned} \vec{\omega}_a &= -\frac{q}{m} \left[a_\mu \vec{B} - a_\mu \left(\frac{\gamma}{\gamma + 1} \right) (\vec{\beta} \cdot \vec{B}) \right. \\ &\quad \left. - \left(a_\mu - \frac{1}{\gamma^2 - 1} \right) \frac{\vec{\beta} \times \vec{E}}{c} \right] \end{aligned}$$

For muons at magic momentum ($p_{mag} = m^2/a_\mu$) circulating on the design orbit, the equation reduces to $\vec{\omega}_a = -\frac{q}{m} a_\mu \vec{B}$. Vertical oscillations will contribute to our measurement of the anomalous precession through the second term in Eq. 1, the so-called pitch correction. The measured distribution of vertical phase space is used to compute the size of the effect. Such a measurement is shown in Fig. 13

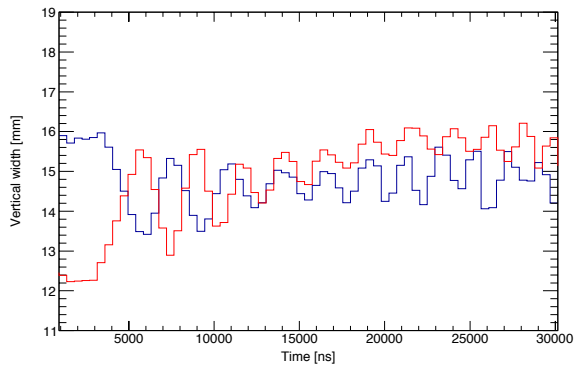


Figure 13: Evolution of the vertical width over the first $30 \mu\text{s}$ of the fill.

The E-field systematic is associated with the third term on the right hand side of Eq. 1 and scales with momentum offset and radial electric field. The electric field depends in turn on transverse displacement. Estimating the size of the E-field systematic depends on measurement of the momentum

and the radial distributions. The radial distribution is measured directly with fiber harps and trackers. The momentum distribution is determined by a fast rotation analysis, that exploits the connection between the revolution frequency and the momentum. A technique [4] based on Fourier transform yields a frequency spectrum that can be correlated with radius (circumference) and momentum. An alternative method extracts the momentum distribution from the measured debunching of the muon beam. The fast rotation data is provided by the calorimeters which measure the time dependence of the intensity of the distribution. Examples of frequency distribution extracted by the Fourier method and radial distribution via the debunching analysis are shown in Fig. 14 and 15 respectively. A radial distribution convoluted with the traceback detector acceptance is shown in Fig. 16.

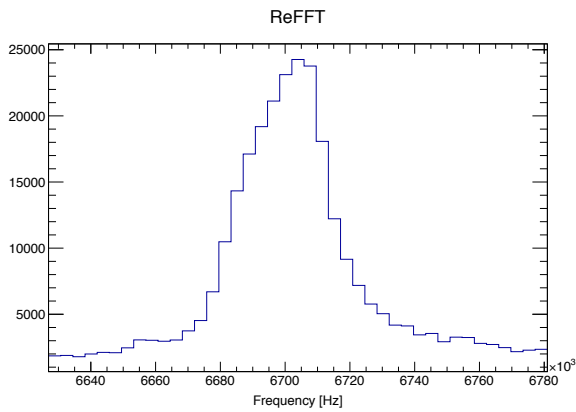


Figure 14: Fourier analysis of the fast rotation signal gives the muon revolution frequency spectrum. Higher frequency corresponds to lower momentum and smaller radius. The revolution frequency of the magic momentum muon is 6.7 MHz.

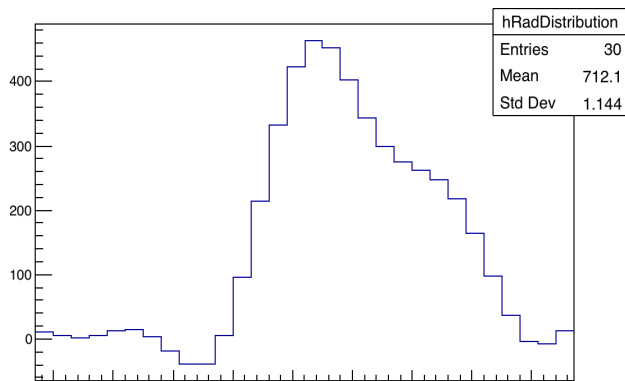


Figure 15: The radial distribution is determined by analysis of the debunching in the fast rotation signal.

The acceptance of the calorimeters for the decay positron depends on the radial position of the parent muon. The acceptance therefore varies as the centroid and width of the distribution evolves over the course of the fill. The coherent motion of the centroid, that results from errors in injection

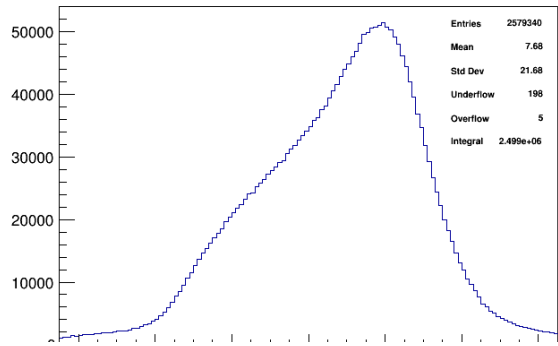


Figure 16: Radial distribution measured with the tracking station.

angle and kicker field, and the coherent modulation of the beam width, arising from the phase space mismatch at injection, are characterized by some decoherence time. (The coherent motion and modulation early in the fill is evident for example in Fig. 5 and 6.) The beam decoheres because of the amplitude and momentum dependence of tunes associated with quadrupole nonlinearity (discussed above) and the chromaticity. But the leading source of decoherence is the large momentum spread and the strong dependence of path length on momentum. The fractional change in circumference due to fractional momentum offset is $\frac{\Delta C}{C} \sim \frac{\eta}{R} \frac{\Delta p}{p} \Rightarrow \Delta p/p$ in the weak focusing limit. The momentum acceptance of the ring is $\Delta p/p \sim \pm 0.125\%$. The distribution overlaps itself in about four hundred turns or 60 μs , effectively mixing the distribution. Indeed a measure of the decoherence time is an indication of the width of the momentum distribution.

The phase space volume of the injected muon distribution overwhelms the ring acceptance. As a result, the distribution that is stored fills the aperture. Muons at the edge of the momentum or transverse aperture may be lost over the course of a fill. If those losses correlate with any particular region of the muon phase space or polarization, there will be a systematic distortion on the measurement of momentum and/or phase space distribution and/or ω_a phase.

In order to insure that all circulating muons are well within the aperture defined by the collimators, muons at the edge of the aperture are scraped at the start of the fill. The scraping is accomplished by adjusting the voltages on the quadrupole plates asymmetrically, thereby introducing an electrostatic dipole moment, that displaces the closed orbit by about 2mm both vertically and radially from the center of the aperture. The asymmetric voltages are sustained for 7 μs (many betatron periods) and then the closed orbit is restored adiabatically. The vertical displacement of the distribution is measured by the traceback detectors (see Fig. 17) at a point in the ring 180 deg beyond the injection point and over the course of the scraping cycle. The remaining distribution on the restored closed orbit will nominally have at least 1mm clearance with respect to the collimators. Muons that are lost are identified as a double (or triple) coincidence in

adjacent calorimeters so that the effectiveness of the scraping procedure can be confirmed.

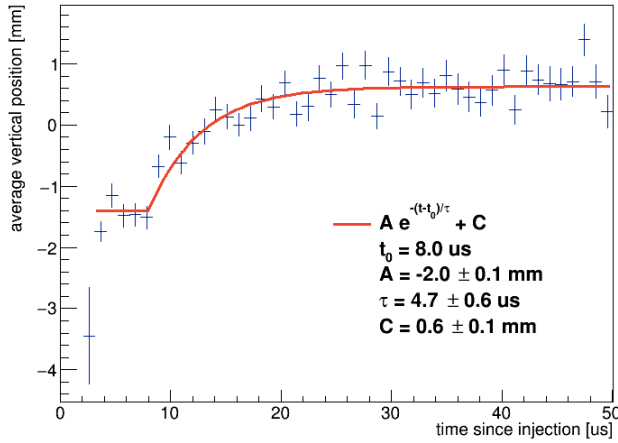


Figure 17: Vertical displacement of the centroid at the 180 deg tracker during the scraping cycle.

CONCLUSION

A quantitative understanding of the evolution of the distribution during the course of the fill is essential to limiting the systematic uncertainty in the measurement of the anomalous magnet moment to the 70 ppb target. The experiment is equipped with detectors that can measure phase space and momentum distribution in some detail, as we have demon-

strated with a few examples. Beam dynamics simulations informed by the measurements complete the description. The data presented above was collected during the commissioning phase of the experiment. As such all results should be considered preliminary. Nevertheless it is clear that the fiber harp and tracker systems are an extraordinary window on the behavior of the circulating distribution.

ACKNOWLEDGEMENT

We would like to thank the Fermilab Research Alliance LLC and the Department of Energy for supporting this research. We acknowledge our Muon g-2 collaborators who have made this experiment and these measurements possible and with whom I have benefited from countless discussions.

REFERENCES

- [1] Muon g-2 Technical Design Report, FERMILAB-DESIGN-2014-02, arXiv:1501.06858.
- [2] D. Sagan, "Bmad: A relativistic charged particle simulation library," *Nucl. Instr. Meth. A*, vol. 558, pp. 356–359, 2006.
- [3] A. P. Schreckenberger et al., "New Fast Kicker Results from the Muon g-2 E-989 Experiment at FERMILAB", presented at the 2018 Int. Particle Accelerator Conf. (IPAC'18), Vancouver, Ca, Ma 2017, paper ,this conference
- [4] Yuri Orlov, Cenap S. Ozben, and Yannis K. Semertzidis, "Muon revolution frequency distribution from a partial-time fourier transform of the g-2 signal in the muon g-2 experiment" *Nucl. Instrum. Methods Phys. Res. A*, 482:9, 2002.
- [5] Y. Semertzidis, et al., "The Brookhaven muon (g-2) storage ring high voltage quadrupoles" *Nucl. Instr. Meth. A*, vol. 503, pp. 458-484, 2003.